PCCP

Accepted Manuscript

This is an *Accepted Manuscript*, which has been through the Royal Society of Chemistry peer review process and has been accepted for publication.

Accepted Manuscripts are published online shortly after acceptance, before technical editing, formatting and proof reading. Using this free service, authors can make their results available to the community, in citable form, before we publish the edited article. We will replace this *Accepted Manuscript* with the edited and formatted *Advance Article* as soon as it is available.

You can find more information about *Accepted Manuscripts* in the Information for Authors.

Please note that technical editing may introduce minor changes to the text and/or graphics, which may alter content. The journal's standard Terms & Conditions and the Ethical guidelines still apply. In no event shall the Royal Society of Chemistry be held responsible for any errors or omissions in this *Accepted Manuscript* or any consequences arising from the use of any information it contains.

PCCP

ARTICLE

Mesomorphism and electrochemistry of thienoviologen liquid crystals

S. Cospito,*[a,b] A. Beneduci,*[a] L. Veltri, [a] M. Salamonczyk,[c] and G. Chidichimo[a]

The thienoviologens series 4,4'-(2,2'-bithiophene-5,5'-diyl)bis(1-alkylpridinium)X_2, **mVX_2** with **X** = counterion is a new class of electron acceptor materials which show very interesting electrochromic and electrofluorescent properties. Depending on the length, m, of the promesogenic alkyl chains, and on the counterion, thienoviologens might became liquid crystals. Here, we present the mesomorphic behaviour, and the electrochemical and spectroelectrochemical properties in solution of new thienoviolgens of the series **mVI_2** and **$mV(NTf_2)_2$** (I = iodide; NTf_2^- = bis(tri-fuoromethylsulfonyl)imide) with m = 8, 12. Interestingly, we found that only the compounds **$12VX_2$** are liquid crystals, exhibiting a calamitic behaviour in contrast to the homologous compounds of the series with m = 9-11 and X = NTf_2^-, which showed columnar rectangular mesophases.

The electrochemical study here reported, allowed us to explain for the first time the anomalous behaviour of these thienoviologens already observed in cyclic voltammetry, where two apparently irreversible redox processes occur. This can be explained by a comproportionation reaction in which the neutral species rapidly reduces the dication to the radical-cation, due to its strong reducing power.

Electrochemical reduction of the thienoviologens causes electrochromism since a new absorption band, occurring at 660 nm in the electronic spectra, growth with the negative potential bias applied. With a LUMO level of 3.64 eV, similar to those of the C_{60} and of other n-type materials, these compounds can find applications in several electronics devices, where their liquid crystalline properties can be used to control film morphology and geometry, provided if they would have good electron mobility.

Introduction

Ionic liquid crystals (ILCs) are a class of liquid-crystalline compounds that contain anions and cations and can be considered as materials that combine the properties of liquid crystals and ionic liquids.[1] Such materials are able to form nanostructured and well defined ion channels, leading to anisotropic ionic conductivity, which is essential for the development of energy devices such as dye-sensitized solar cells,[2-5] batteries[6-7] and ion transistors.[8] Monomeric ILCs with charged side chains, with charged aromatic cores or charged group directly attached to the core were extensively investigated.[9] Liquid crystals salts with an extended π-conjugated and electroactive core, represent a new generation of nanostructured electrochromic (EC) materials with 1D or 2D pathways for ionic and electronic charges.[10-12] Redox active liquid crystals, without any ionic function, do not show electrochromism in the bulk state but only in electrolyte solutions.[13-15] Therefore, efficient solid state EC devices can be easily assembled incorporating a single layer of ILC material between two transparent conductive electrodes. Bipyridinium salts, also known as viologens, are the most famous electrochromes, used as cathodic colouring component in EC devices.[16-18] Viologen-based liquid crystals deserve particular attention and a wide range of their derivatives were synthesized showing either smectic[19-22] or columnar[23,24] phase. The extension of

the π-conjugation between the two pyridinium units, by means aromatic groups, allows to modulate the electrochemical and spectroelectrochemical response of new electron acceptor conductors, known as extended viologens.[25-28] Such compounds, in which electron acceptor groups are connected by electron rich heterocyclic oligomers, are typical acceptor-donor-acceptor (A-D-A) molecular wires.[29] In particular, if an oligothiophene moiety is inserted between two pyridinium rings, the resulting compounds are called thienoviologens. Albers and co-workers proposed new biosensors based on the functionalization of electrode surfaces with self-assembled thienoviologens able to create an electronic communication between redox enzymes and the electrode.[30-31] Thienoviologens are also well known for their strong photoluminescence,[25] and this property coupled to the meomorphism, as recently demonstrated, gave rise to new multifunctional materials.[12] Extended viologens containing a bithiophene unit 4,4'-(2,2'-bithiophene-5,5'-diyl)bis(1-alkylpridinium)bis(tri-fuoromethylsulfonyl)imide, **$(mV(NTf_2)_2)$**, where the alkyl-chain length (m) was 9-11 carbon atoms, were synthesized,[32] and proposed as the first example of electrofluorochromic liquid crystals.[12] As shown, these materials are able to reversibly modulate both their absorption colour (electrochromism) and their fluorescence (electrofluorochromism)

upon electrochemical reduction.[12] These interesting properties are affected by the nature of the mesophase which, in turn, is determined by the alkyl chain length m.[32] Moreover, we pointed out that the anion plays a crucial role in disclosing the liquid crystalline nature of the thienoviologen dications mV^{++}.[32] Indeed, we found that the mesogens $mV(NTf_2)_2$ self-assemble into columnar or smectic phase, while their precursors with iodide as anion, did not show any mesomorphism. [32] Thus, with the aim to better understand the effect of the alkyl-chain length on the nature of the mesophases, here, we propose new thienoviologens with m = 8 and 12, expanding the ($mV(NTf_2)_2$) series previously reported.[32] These compounds were fully characterized either for their mesomorphism or for their electrochemistry in solution phase.

Experimental

Synthesis of mesogens

Synthesis of 4,4'-(2,2'-Bithiophene-5,5'-diyl)bis(1-octylpyridinium) iodide ($8VI_2$) and 4,4'-(2,2'-Bithiophene-5,5'-diyl)bis(1-dodecylpyridinium) iodide ($12VI_2$)

In a Schlenk flask, 5,5'-bis(4-pyridyl)-2,2'-bithiophene 1[33] (1 g, 3.12 mmol) was suspended under a nitrogen atmosphere in 70 mL of anhydrous chloroform. To the stirred suspension was added the appropriate iodoalcane (31.2 mmol) [iodododecane: 7.49 g; iodododecane: 9.24 g] and the mixture was heated at 80°C for 24 h. After cooling, the solvent was removed under vacuum and to the resulting mixture was added diethyl ether (50 mL). The suspension was filtered, and the solid residue was washed several times with diethyl ether (6 X 10 mL) to give pure $8VI_2$ and $12VI_2$.

4,4'-(2,2'-Bithiophene-5,5'-diyl)bis(1-octylpyridinium) iodide ($8VI_2$). Yield: 1.80 g, starting from 1 g of 1 (72%). Orange solid, mp 183-185 °C. IR (KBr): ν = 2932 (m), 1639 (s), 1530 (m), 1434 (m), 1227 (m), 1082 (m), 803 (m), 618 (w) cm^{-1};^{1}H NMR(300 MHz, CDCl$_3$): δ = 9.05 (d, J = 5.9, 4H,H-2 + H-2' + H-6 + H-6' on pyridine rings), 8.23 (d, J=5.9, 4 H,H-3 + H-3'+ H-5 + H-5' on pyridine rings), 7.99 (d, J =4.2, 2 H, H-3 + H-3' on thiophene rings), 7.22 (d, J = 4.2, 2 H, H-4 + H- 4' on thiophene rings), 4.71 (t, J = 7.4, 4 H, 2 $^+$NCH_2CH$_2$(CH$_2$)$_5$CH$_3$), 2.09–1.95 (m, 4 H, 2 $^+$NCH$_2$CH_2(CH$_2$)$_5$CH$_3$), 1.45–1.12 (m, 20 H, 2 $^+$NCH$_2$CH$_2$(CH_2)$_5$CH$_3$), 0.87 (t, J = 7.3, 6 H, 2 $^+$NCH$_2$CH$_2$(CH$_2$)$_5$CH_3); anal. calcd for C$_{34}$H$_{46}$I$_2$N$_2$S$_2$ (800.68): C 51.00, H 5.79, I 31.70, N 3.50, S 8.01; found C 51.16, H 5.80, I 31.79, N 3.49, S 7.98.

4,4'-(2,2'-Bithiophene-5,5'-diyl)bis(1-dodecylpyridinium) iodide ($12VI_2$). Yield: 2.27 g, starting from1 g of 1 (80%). Orange solid, mp 240-241 °C. 2931 (m), 1639 (s), 1529 (m), 1433 (m), 1227 (m), 1088 (m), 815 (m), 577 (m); ^{1}H NMR(500 MHz, CDCl$_3$): δ = 9.04 (d, J = 6.6, 4H,H-2 + H-2' + H-6 + H-6' on pyridine rings), 8.24 (d, J=6.6, 4 H,H-3 + H-3'+ H-5 + H-5' on pyridine rings), 7.99 (d, J =4.1, 2 H, H-3 + H-3' on thiophene rings), 7.22 (d, J = 4.1, 2 H, H-4 + H- 4' on thiophene rings), 4.71 (t, J = 7.4, 4 H, 2 $^+$NCH_2CH$_2$(CH$_2$)$_6$CH$_3$), 2.09–1.98 (m, 4 H, 2 $^+$NCH$_2$CH_2(CH$_2$)$_9$CH$_3$), 1.48–1.19 (m, 36 H, 2 $^+$NCH$_2$CH$_2$(CH_2)$_9$CH$_3$), 0.87 (t, J = 6.8,6 H, 2 $^+$NCH$_2$CH$_2$(CH$_2$)$_9$CH_3); anal. calcd for C$_{42}$H$_{62}$I$_2$N$_2$S$_2$ (912.89): C 55.26, H 6.85, I 27.80, N 3.07, S 7.02; found C 55.31, H 6.86, I 27.88, N 3.06, S 7.05%.

Synthesis of 4,4'-(2,2'-Bithiophene-5,5'-diyl)bis(1-octylpyridinium) triflimide ($8V(NTf_2)_2$) and 4,4'-(2,2'-Bithiophene-5,5'-diyl)bis(1-dodecylpyridinium) triflimide ($12V(NTf_2)_2$)

To a stirred solution of viologen iodide (1mmol) [$8VI_2$: 0.8 g; $12VI_2$: 0.92 g;] in 300 mL of methanol was added lithium triflimide (1.15 g;

4 mmol). The mixture was stirred at room temperature for 15 h. The solvent was removed under vacuum and to the resulting mixture was added water (50 mL). The suspension was filtered, and the solid residue was washed several times with water (4 X 10 mL) to give pure $8V(NTf_2)_2$ and $12V(NTf_2)_2$.

4,4'-(2,2'-Bithiophene-5,5'-diyl)bis(1-octylpyridinium) triflimide ($8V(NTf_2)_2$). Yield: 0.876 g, starting from 0.8 g of $8VI_2$ (79%). Yellow solid, mp123-126°C. IR (KBr): ν = 2930 (m), 1637 (s), 1529 (m), 1434 (m), 1361 (s), 1209 (s), 1138 (m), 1056 (m), 808 (m), 615 (s) cm^{-1}; ^{1}H NMR (300 MHz, DMSO-d$_6$): δ = 9.00 (d, J = 6.3, 4 H, H-2 + H-2' + H-6 + H-6' on pyridine rings), 8.40 (d, J = 6.3, 4 H, H-3 + H-3' + H-5 + H-5' on pyridine rings), 8.34 (d, J = 3.9, 2 H, H-3 + H-3' on thiophene rings), 7.87 (d, J = 3.9, 2 H, H-4 + H-4' on thiophene rings), 4.51 (t, J = 7.0, 4 H, 2 $^+$NCH_2CH$_2$(CH$_2$)$_5$CH$_3$), 1.99 – 1.85 (m, 4 H, 2 $^+$NCH$_2$CH_2(CH$_2$)$_5$CH$_3$), 1.39–1.17 (m, 20 H, 2 $^+$NCH$_2$CH$_2$(CH_2)$_5$CH$_3$), 0.86 (t, J = 6.8, 6 H, 2 $^+$NCH$_2$CH$_2$(CH$_2$)$_5$CH_3); ^{19}F NMR (471 MHz, DMSO-d$_6$): δ = -78.3 (s, 3 F, CF$_3$); MS (ESI+, direct infusion): m/z = 400 [M – 2 NTf$_2^-$]$^{2+}$; anal. Calcd for C$_{38}$H$_{46}$F$_{12}$N$_4$O$_8$S$_6$ (1107.16): C 41.22, H 4.19, F 20.59, N 5.06, S 17.38; found C 41.28, H 4.18, F 20.61, N 5.07, S 17.40.

4,4'-(2,2'-Bithiophene-5,5'-diyl)bis(1-dodecylpyridinium) triflimide ($12V(NTf_2)_2$). Yield: 0.915 g, starting from 0.92 g of $12VI_2$ (75%). Yellow solid, mp 192-193°C. IR (KBr): 2927 (m), 1638 (s), 1528 (s), 1436 (m), 1353 (s), 1205 (s), 1173 (s), 1138 (m), 1059 (m), 736 (w), 651 (m) cm^{-1}; ^{1}H NMR (500 MHz, DMSO-d$_6$): δ = 9.01 (d, J = 6.0, 4 H, H-2 + H-2' + H-6 + H-6' on pyridine rings), 8.40 (d, J = 6.0, 4 H, H-3 + H-3' + H-5 + H-5' on pyridine rings), 8.35 (d, J = 3.7, 2 H, H-3 + H-3' on thiophene rings), 7.87 (d, J = 3.7, 2 H, H-4 + H-4' on thiophene rings), 4.52 (t, J = 6.7, 4 H, 2 $^+$NCH_2CH$_2$(CH$_2$)$_9$CH$_3$), 1.97 – 1.87 (m, 4 H, 2 $^+$NCH$_2$CH_2(CH$_2$)$_9$CH$_3$), 1.39–1.14 (m, 36 H, 2 $^+$NCH$_2$CH$_2$(CH_2)$_9$CH$_3$), 0.85 (t, J = 6.4, 6 H, 2 $^+$NCH$_2$CH$_2$(CH$_2$)$_9$CH_3); ^{19}F NMR (471 MHz, DMSO-d6): δ = -78.3 (s, 3 F, CF$_3$); MS (ESI+, direct infusion): m/z = 329 [M – 2 NTf$_2^-$]$^{2+}$; anal. Calcd for C$_{46}$H$_{62}$F$_{12}$N$_4$O$_8$S$_6$ (1219.38): C 45.31, H 5.12, F 18.70, N 4.59, S 15.78; found C 45.49, H 5.10, F 18.68, N 4.60, S 15.81.

Measurements

Melting point analyses were performed on a Linkam (LTS350 stage, TP94 System Controller) at a scan rate of 10 °C min^{-1}. ^{1}H-NMR spectra were recorded at 25°C in CDCl$_3$ or DMSO-d$_6$ on an Avance 300 Bruker NMR spectrometer at 300 MHz or on an Avance 500 Bruker NMR spectrometer at 500 MHz with Me$_4$Si as an internal standard. 19F NMR spectra were recorded at 25°C in DMSO-d$_6$ on an Avance 500 Bruker NMR spectrometer at 471 MHz with CFCl$_3$ as an internal standard. Chemical shifts ($δ$) and coupling constants (J) are given in ppm and in Hz, respectively. IR spectra were taken with a JASCO FT-IR 4200 spectrometer. Microanalyses were carried out with a Carlo Erba Elemental Analyzer Mod. 1106. Mass spectra were obtained using an ABSciex API 2000 mass spectrometer equipped with a turbo ion spray ionization source in the positive mode (ion spray voltage 4500 V; curtain gas 10 psi; temperature 25°C; ion source gas 20 psi; declustering and focusing potentials 50 and 400 V, respectively).

Polarizing optical microscopy (POM)

Mesophases were identified by observation of sample microscopic textures using a Leitz Laborlux 12 POL polarising optical microscope in conjunction with a Linkam LTS350 heating stage.

Differential scanning calorimetry (DSC)

Phase transition temperatures and enthalpy changes were determined by differential scanning calorimetry (DSC) measurements performed with a TA DSC Q200 set-up in inert atmosphere with scan rate 10 °C min^{-1}.

X-ray diffraction (XRD) analysis

The powder X-ray diffraction patterns at variable temperatures were obtained using a Bruker Nanostar system with Cu Kα radiation (SAXS measurements) and Bruker GADDS system (point collimated Cu Kα radiation, Vantec 2000 area detector).

Electrochemistry

The electrochemical behaviour of *12V(NTf$_2$)$_2$* (0.5 mM) was investigated by cyclic voltammetry (CV) in Propylen carbonate (PC) degassed solution containing tetrabutylammonium-hexafluorophosphate (TBAPF$_6$) 0.1 M as electrolyte. The measurements were done at a glassy carbon disc working electrode in a three-electrode cell, using a platinum auxiliary electrode, an Ag/AgCl reference electrode and a potentiostat configuration from AMEL s.r.l. (Mod. 7050). All the potentials were calibrated against the Fc/Fc$^+$ couple (0.5 mM).

Spectroelectrochemistry

Spectroelectrochemical experiments was conducted in an electrolytic cell (BioLogic Science Instruments) which was composed of a 1 mm cuvette, where a platinum gauze thin layer and a platinum wire were used as working electrode and auxiliary electrode, respectively. A pseudo-reference electrode consisted of an Ag wire was calibrated against the Fc$^+$/Fc redox couple. The spectroelectrochemical cell was filled with a solution containing 1 mM of *12V(NTf$_2$)$_2$* and TBAPF$_6$ (0.1 M) dissolved in PC. UV–vis–NIR spectra were recorded with a Jasco V-550 UV–vis spectrophotometer. The potential was supplied by means of an Amel 2049 model potentiostat. Measurements were performed at 25°C.

Results and discussion

Synthesis and Mesomorphic properties

Both thienoviologens, *8V(NTf$_2$)$_2$* and *12V(NTf$_2$)$_2$* (Fig. 1a) were synthesized following the synthetic procedure, already used for the *mV(NTf$_2$)$_2$* with m= 9-11 (Fig S1).[32,33]
We investigated the mesomorphism of both *mV(NTf$_2$)$_2$* and its *mVI$_2$* precursors by polarizing optical microscopy (POM), differential scanning calorimetry (DSC) and X-ray diffractometry (XRD). This analysis revealed a liquid crystalline behaviour for both the compound with m = 12. The DSC trace of *8V(NTf$_2$)$_2$* in Fig. S2, shows two peaks in the first heating scan at 50 °C and 125 °C. In this range none of the typical textures of mesophases is observed at POM, indicating that at 50 °C only a structural rearrangement between crystalline phases occurs, as confirmed in the second heating scan, where only the melting peak at 125 °C appears.
Fig. 1(a) shows the DSC diagram of *12V(NTf$_2$)$_2$* in the first thermal cycle. In the first heating scan a first broad endothermic peak with a large enthalpy change (11.15 J/g) occurs at 43 °C. POM observation of a thin film of *12V(NTf$_2$)$_2$*, did not show any significant change in the texture. Moreover, the material was still hard, indicating that this enthalpy change could be due to a crystal to crystal phase transition. At about 121 °C a very intense (ΔH =28.87 J/g) and sharp peak appears on the thermogram and the material become soft, suggesting the formation of a liquid crystalline phase, whose birefringence

texture is shown in Fig. S3(a). By increasing the temperature, another broad peak at 167 °C (ΔH =5.55 J/g) was recorded and a focal conic texture appears (Fig. S2(b)), which was observed up to the isotropic liquid state (IL), occurring above 180 °C (ΔH =4.39 J/g).

(a)

8VX: R=(CH$_2$)$_7$CH$_3$ X = I or NTf$_2$
12VX: R = (CH$_2$)$_{11}$CH$_3$

(b)   (c)
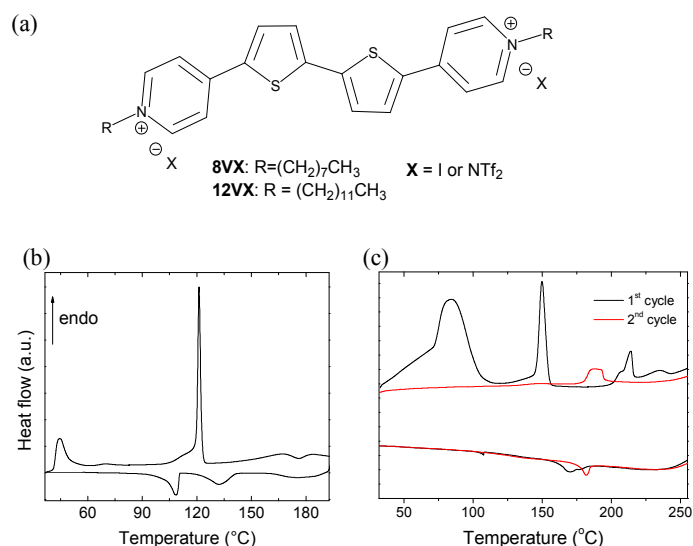
Fig. 1 Chemical structure of the thienoviologen liquid crystals *mVX$_2$* (a) and the DSC traces of *12V(NTf$_2$)$_2$* for the 1st thermal cycle (b), and of *12VI$_2$* for the first two thermal cycles (c). Scan rate 10 °C min^{-1}.

When cooled from the melt, bâtonnets started to form (Fig. 2(a)), which then transformed into the typical fan-shaped texture of a smectic phase (Fig. 2(b)). Upon further cooling across the second transition found by DSC (about 132 °C, ΔH =6.65 J/g)), striated fan-shaped textures were observed (Fig. S3(c)). At about 108 °C another low enthalpy (6.47 J/g) transition led to solidification (Fig. S3(d)) and no further changes were detected down to room temperatures.

(a)   (b)

(c)
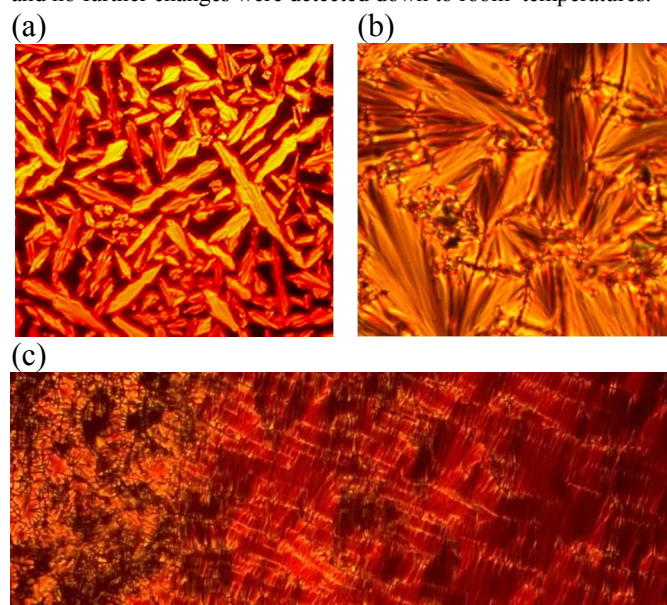
Fig. 2 Optical textures of a thin film of *12V(NTf$_2$)$_2$* between two glass slides under cross polarized, upon cooling from the IL state

scan at (a) 185 °C and (b) 170 °C and of *12VI₂* upon cooling from IL state at (c) 240 °C.

Fig. 1(b) shows the DSC trace relative to compound *12VI₂*. On the first heating scan, its thermal behaviour is qualitatively similar to that just described for the corresponding bistriflimide thienoviologen, with a broad peak at 84 °C (ΔH = 45.36 J/g) and a sharp intense peak at 150 °C (ΔH =17.22 J/g). Above this last transition, the material became soft suggesting the formation of a liquid crystalline phase. On further heating above 240 °C, the compound starts decomposing. In order to prevent compound degradation, the sample was fast heated close to its clearing temperature (about 255 °C as determined by POM) and introduced by capillarity into a sandwich cell when it was still in the mesophase. Interestingly, large domain of smectic phase oriented along the filling direction spontaneously formed inside the cell, where the oriented smectic layers are arranged in long filaments across the whole cell area (Fig.S4(a)). A typical polydomains fan-shaped focal conics texture was instead observed outside the sandwich (Fig. 2(c)). The above self-assembled aligned structure was kept unaltered down to room temperature, suggesting the possibility to use this filling method to prepare highly oriented films of these LC materials for optoelectronics. In the second heating scan, large areas of the sample were brought to the IL state just above 255 °C. However, in order to prevent sample decomposition, it was kept at the clearing temperature for a few seconds and then cooled again at 5 °C/min. At 240 °C, bâtonnetes formed in the dark areas of the sample (Fig. S4(b)), that coalesced into not aligned fan shaped domains, on further cooling (Fig. S4(c)). Notably, some aligned smectic domains could be still observed in those areas of the sample where no clearing occurred (Fig. S4(c)).

Compound decomposition was confirmed by DSC which showed only a broad peak in the first cooling scan (at about 175 °C), the loss of all the endothermic peaks observed in the first heating scan, and the appearance of a broad peak at about 190 °C in the second heating scan (Fig. 2b).

The mesomorphism observed at POM was also investigated by variable temperature X-ray diffractometry. Fig. S5(a) displays the X-ray diffraction pattern of *12V(NTf₂)₂* at 140 °C in the first heating scan, that confirm the tendency for this thienoviologen salt as well as for the others already studied[32] to self-assemble into rectangular columnar phase (Col_r). The sample gave three sharp diffraction signals in the small angle region that can be indexed as (11), (20) and (31) (Fig. S5(b)). The signal positions were almost temperature independent. We proposed a dimerization of the cations through bridging interacting anions, that gives rise to a disc-like structure, with the rigid cores having an elliptical cross section, and the alkyl chains constituting the fringes (Fig. S5(c)).[32] Molecular modeling of the dimer gave elliptic shape with diameters ca. 20 and 42 Å, while the unit cell parameters, calculated from X-ray measurement, are a = 34.1 Å and b = 54.9 Å at 125 °C. This indicates significant interdigitation of the alkyl chains between neighboring columns. Distortion from the hexagonal structure measured as ratio of unit cell parameters b/a = 1.6 was found. These elliptic dimers self-assemble in columns packed parallel on a two-dimensional rectangular lattice with C2/m symmetry (Fig. S5(c)).

Increasing the temperature, the X-ray pattern recorded at 180 °C showed a series of sharp, commensurate Bragg reflections which proves clearly that the molecules organize into a lamellar phase with a measured interplanar distance of 35 Å (Fig. 3). At the high angle region of the X-ray pattern the diffused signal, characteristic for short range positional order between molecules, was detected.

By taking into account the POM observations and that the length of the dication *12V⁺⁺*, calculated in their maximum elongation with all

trans chain conformation, is about 45 Å, it is possible to propose a smectic A (SmA) mesophase, with a high degree of interdigitation between alkyl chains.

On the other hand the X-ray diffraction analysis performed on cooling from the melt showed the typical X-ray pattern of a SmA mesophase at 150 °C that frozen at 123°C into a glassy phase before crystallization below 108 °C. The layer spacing of the SmA phase is 34 Å and is similar to the distance measured on heating. However, in the subsequent thermal cycle, no columnar phase was observed in either POM or XRD and the material self-assembled directly into the smectic A phase.
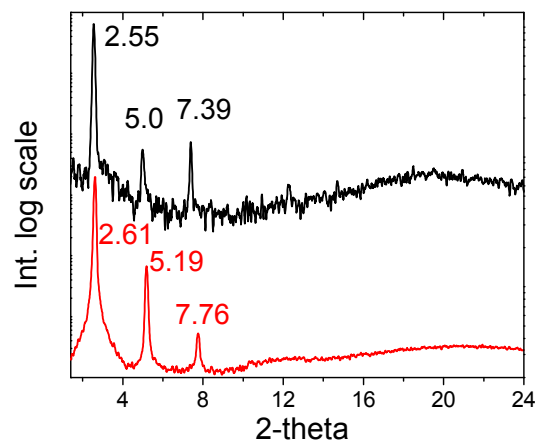
Fig. 3 XRD diffractograms of *12V(NTf₂)₂* recorded at 180 °C on the 1ˢᵗ heating scan (black) and at 130 °C on the 1ˢᵗ cooling scan (red).

Mesomorphism of *12VI₂* is very similar to that of *12V(NTf₂)₂* described above, showing also a SmA phase (Fig.S6). In this case, however, the layer distance is 36.2 Å and is much shorter than the length of the straight dication (ca. 45 Å). Therefore, a higher alkyl chains interdigitation was found.

In summary, here we can highlight the crucial effects played by both the length of the alkyl chain and the type of anion. Indeed, of the series *mVI₂* with m = 8-12, only the compound with the longest chain exhibits liquid crystalline properties. In contrast, all the compounds of the series *mV(NTf₂)₂* are liquid crystals except that with the shortest chain. Of the two series, the iodides have higher clearing points than the bistriflimide homologous compounds (Fig. S7). Moreover, the liquid crystal *12VI₂* has a higher crystal-to-mesophase transition temperature than the *12V(NTf₂)₂* compounds. These differences are essentially due to the larger dimension of the bistriflimide anion, the alkyl chain length being the same. Similar considerations have been already reported on ionic liquid crystals based on the imidazolium ion *N*-substituted with large aromatic moieties. It has been shown that, with increasing anionic radius, the clearing point decreases and the mesophase range is extended below room temperature by shifting the Liquid crystal-Crystal transition point.[34]

There is an interesting interplay between the soft moiety of the dication and the counterion, which leads to different structural properties and that, in the case of the thienoviologen bistriflimides, determines the way these compounds self-assemble.

Figure 4 clearly displays the effect of the alkyl chain length on the mesomorphic behaviour of the thienoviologens *mV(NTf₂)₂*. The columnar arrangement is stable at lower *m* and lower temperatures, while the calamitic behaviour is the preferred organization at higher *m* and higher temperatures. The columnar phase is definitely lost for *m* = 12, after the first heating scan, indicating that the longer chains in this case do not allow for disc formation through cation

dimerization (Fig. S5(c)), probably because of a larger steric hindrance. Fig. 4 shows also that, while the transition temperature into the isotropic liquid state increases with *m*, the onset temperature of the mesophase on heating, changes only slightly in the series and does not show a monotonic trend. That results in a significant increases of the range of existence of the mesophase, from about 12 °C to about 65 °C, with the length of the alkyl chain, i.e., with the increase of the soft portion of the compounds.
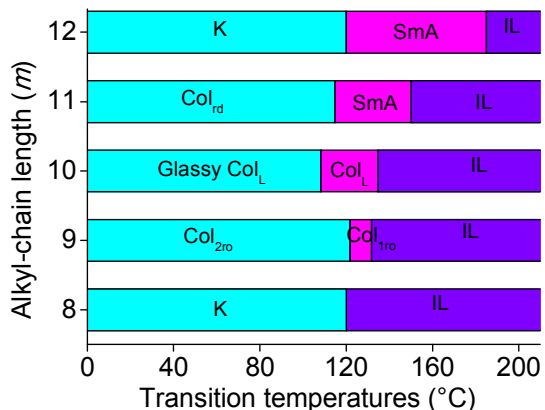
Fig. 4 Phase diagram of *mV(NTf₂)₂* with m = 8-12 in the 2nd heating scan; abbreviations: K = crystalline solid, Col_{rd} and Col_{ro} = disordered and ordered columnar rectangular phases, respectively, Col_L = lamello-columnar phase, SmA = smectic A phase, IL = isotropic liquid state.

Electrochemistry

The electrochemical properties of the thienoviologens in solution were investigated by cyclic voltammetry (CV). The CV diagrams in Fig. 5, reveal the electron-acceptor nature of the thienoviologen dication salt (TV^{+2}).[12,25,35] Indeed, at 30 mV/s the voltammetry displays two reduction peaks due to the formation of the radical-cation $TV^{+\bullet}$ and the neutral TV species, respectively, at negative half-wave potentials of -0.75 V and -0.96 V vs Ag/AgCl. It can be seen that, at this scan rate, while the current ratio between the cathodic and anodic peak (ip_c/ip_a) relative to the first redox process ($TV^{+2}/TV^{+\bullet}$) is less than unity, the ip_c/ip_a relative to the second redox couple ($TV^{+\bullet}/TV$) is much larger than unity. Nevertheless, the electrochemical cycle is fully reversible even after several scans. This interesting behaviour has been already observed so far in analogous experimental conditions.[35,36] However, a quantitative study aimed at the comprehension of this behaviour has never been performed and, therefore, a clear explanation of the electrochemistry of thienoviologens in solution has never been provided.

The ip_c/ip_a ratios cited above strongly depend on the scan rate, as shown in Fig. 5 and Fig. S8. As this is increased, both ratios tend to unity, indicating that a reversible behaviour can be reached at high scan rates. This trend can be explained by recalling that viologens undergo a comproportionation reaction in aqueous solutions.[16] Despite this reaction has never been observed in organic solvents, here we have clear evidence that in propylene carbonate (PC) and other polar organic solvents (NMP, DMF DMAc), the neutral thienoviologen TV, a highly reducing species, does indeed reacts with the dication coming from the bulk near the electrode, generating two moles of the $TV^{+\bullet}$ species per mole of TV (eqn. 1):[36]

$$TV + TV^{+2} \rightarrow 2\ TV^{+\bullet} \qquad (1)$$
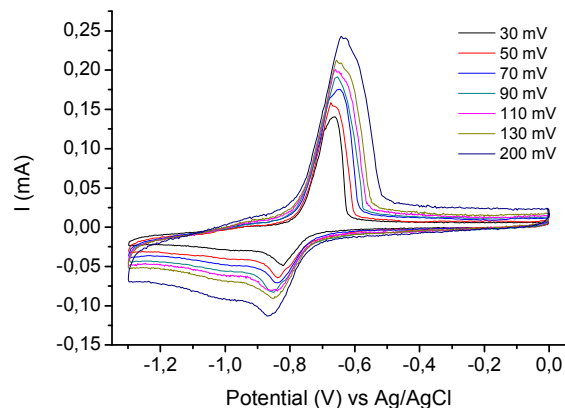
Fig. 5 Cyclic voltammograms at different scan rates of *12V(NTf₂)₂* (0.5 mM) in electrolyte solution PC/0.1 M $TBAPF_6$

At sufficiently low scan rates, most of the neutral species is allowed to react according to the comproportionation reaction in the time interval between its formation at the electrode and its subsequent reoxidation in the oxidative half cycle scan. This leads to a very high ip_c/ip_a ratio, which is proportional to the $[TV^{+\bullet}]/[TV]$ concentration ratio.

(a)

(b)
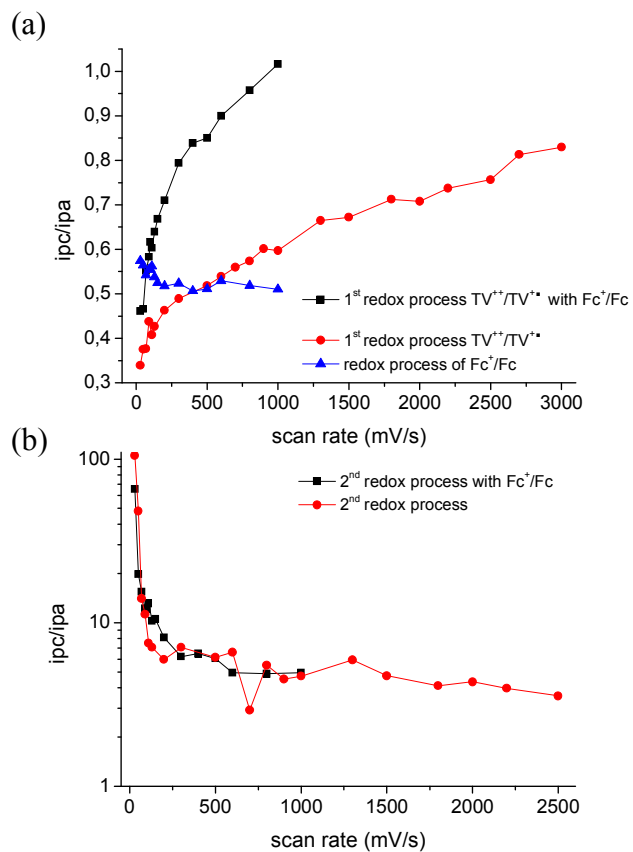
Fig. 6 Plot of the current ratio (ip_c/ip_a) as function of the scan rate for the first (a) and the second redox processes (b).

On the other hand, since the extra amount of radical-cation species formed in the comproportionation reaction (two moles per mole of neutral species), is reoxidized at the electrode, the ip_c/ip_a ratio of the first couple results lower than unity, being it proportional to the $[TV^{+\bullet}]/[TV^{2+}]$ concentration ratio.

At higher scan rates, the time interval occurring between the second reduction peak and the first oxidation peak is reduced and the effect of the comproportionation is less significant. This can be seen from the tendency of the ip_c/ip_a ratios toward unity (Fig. 6).

It is interesting to study the electrochemistry of the thienoviologen when an anodic component is introduced in the electrolytic solution such as ferrocene, which is also a pseudo internal standard and will be used later for calculating the LUMO level.

Fig. S9 reports the CV diagrams of the complementary system that, in addition to the redox waves of the thienoviologen, shows the redox peaks of the Ferrocenium/Ferrocene (Fc^+/Fc) couple occurring at an half wave potential of + 0.40 V *vs.* Ag/AgCl.

Also in this case, we have a low ip_c/ip_a ratio of the first couple and very high ip_c/ip_a ratio of the second couple of thienoviologen. However, as the scan rate is increased the tendency of the first of the above ratio to unity (Fig. 6a black points) is largely increased with respect to that in the absence of ferrocene (Fig. 6a red points) and a $ip_c/ip_a=1$ is obtained just below 800 mV/s. In this case, the comproportionantion reaction comes into a competition with reaction (2) in which the neutral thienoviologen species reacts with the ferrocenium ion to form the radical cation and the ferrocene:

$$TV + Fc^+ \rightarrow TV^{+\bullet} + Fc \qquad (2)$$

Assuming that both the above reactions occur with similar kinetics, it can be argued that this competition leads to an increase of the ip_c/ip_a ratio for the first thienoviologen couple at the same scan rate, since reaction (2) gives only one mole of $TV^{+\bullet}$ per mole of neutral species. On the other hand, under this assumption, the above competition should not introduce significant changes in the behaviour of the ip_c/ip_a ratio for the second thienoviologen couple, since the neutral species is anyway consumed in both reactions. Indeed, the ip_c/ip_a ratio is slightly affected by the introduction of ferrocene in the solution (Fig. 6b).

Moreover, from Fig. 6 it can be seen that the ip_c/ip_a ratio for ferrocene is smaller than one (0.55) and is quite independent on the scan rate (blue plot in Fig. 6a). This ratio is proportional to the $[Fc^+]/[Fc]$ concentration ratio and, in the above hypothesis, $[Fc] > [Fc^+]$.

Spectroelectrochemistry and electronic properties

The electrochromic behaviour of the thienoviologens dissolved in electrolyte solution was investigated by spectroelectrochemistry. Fig. 7 shows the electronic spectra of *12V(NTf₂)₂* obtained upon electrochemical reduction. Without any applied potential (0 V) only a strong absorption band centred at 430 nm due to $\pi\rightarrow\pi^*$ transition is present and the solution appears yellow (inset in Fig. 10). When the potential is negatively increased to -1.2 V *vs.* Fc^+/Fc, the previous peak at 430 nm persists and a new broadband centred at about 660 nm appears, which originates from the radical cation state. This reduction process is accompanied by an obvious colour change from yellow to green (inset in Fig. 7). The electrochromic band grows in intensity, without changes, at more negative potentials at which the second reduction takes place, indicating that the radical-cation is still produced and its concentration increase, despite the neutral species is formed. Thus highlighting the occurrence of the comproportionation reaction.

In order to assess the electron acceptor strength of this class of compounds, we calculated the absolute energy of the HOMO and LUMO levels. Cyclic voltammetry (CV), can be used to provide estimates of the energy levels by carrying out redox reactions compared to an internal redox standard, such as ferrocene.[37]

The onset of the first reduction potential (*vs.* Fc^+/Fc) of the thienoviologen determined by CV (Fig. S9), was used to estimate the LUMO level (E_{LUMO}).[38] Then, assuming that the energy level of ferrocene is 4.8 eV below vacuum level, we calculated the LUMO level of the thienoviologen by using the empirical formula:[39]

$$E_{LUMO} = - E_{onset\ (red)} - 4.8 = (1.162 - 4.8)\ eV = - 3.64\ eV$$
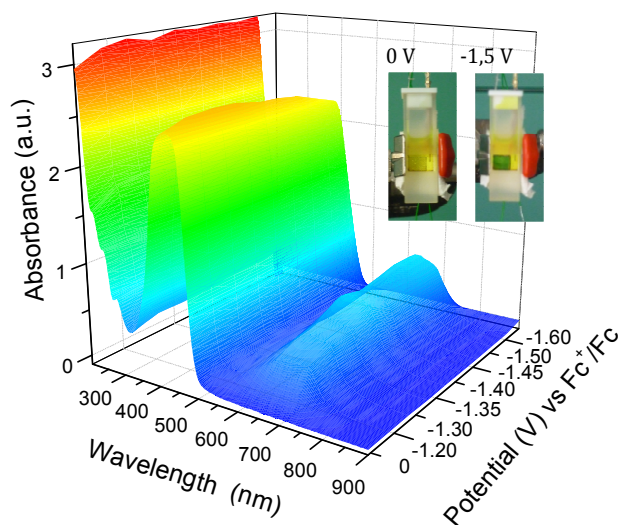
Fig. 7 3D Spectroelectrochromic behaviour of *12V(NTf₂)₂* (1 mM) in PC/0.1 M TBAPF₆ and (inset) visible electrochromism in a spectroelectrochemical cell.

The optical band gap (E_g) was then evaluated from the λ_{onset} of the absorption spectrum (curve at 0 V in Fig. 10)[39] according to the empirical formula:[40] $E_g = 1240/\lambda_{onset} = 2.53$ eV. Thus, the $E_{HOMO} = E_{LUMO} - E_g = (-3.64 - 2.53)\ eV = - 6.44\ eV$.

Interestingly, the LUMO value of the *12V(NTf₂)₂* is very close to that of C_{60} (3.7 eV)[41] which is one of the most common electron acceptors used in organic photovoltaics (OPVs). Therefore, if measurements of charge carrier mobility (currently in progress) confirm the electron transporting attitude of these materials, they could be used in OPV cells as new n-type materials. Indeed, semiconducting LCs seem to be ideal candidates for the preparation of highly ordered heterojunctions for OPVs, due to their ability to self-heal structural defects and to form large single domains (upon thermal annealing).[42-45] In addition, the above properties combined to the strong photoluminescence properties of *mV(NTf₂)₂*, could be used in light emitting electrochemical cells (LECs)[46] where the thienoviologen could play the roles of electronic and ionic semiconductor[47] as well as of fluorescence component.[12] However, in spite of considerable research efforts in this area, n-type organic semiconductors suitable for real-world applications remain rather scarce owing to their often limited stability and poor solubility. For this reason, nowadays only few examples of n-type LCs such as: hexaazatriphenylenes,[48] hexaazatrinaphthylenes,[49] antraquinone,[15,50] tetraazanaphtacene,[51] and perylendiimide.[52-54] have been reported. Therefore, because of their multifunctional properties,[12] thienoviologens can contribute to expand the limited range of n-type

LCs, providing a new class of materials for several applications in organic electronics.

Conclusions

Here we reported a comprehensive study of the mesomorphism of the thienoviologens *mV(NTf₂)₂* as a function of the length of the alkyl chains, *m*. It was found that the shortest length able to obtain liquid crystalline behaviour is of 9 carbon atoms. The parameter *m* strongly affects also the mesomorphism, giving raise to columnar mesophases for shorter chains and smectic phases for longer chains. This bismesomorphic behaviour is due to the stabilization of dimeric units with disc like shape that self-assemble in columnar rectangular aggregates, at shorter m. The longer chains however, destabilize the dimers leading to a calamitic behaviour, as it should be expected taking into account the elongated shape of the thienoviologen dications.

mV(NTf₂)₂ are an important class of electroactive ionic liquid crystals. In particular, they exhibit n-type character, with two reduction processes that lead to the formation of the radical cation and the neutral species. The electrochemical study reported above allowed us to highlight the strong reducing properties of the neutral species that, once formed in solution, rapidly reacts with the dication species to produce the radical-cation. Notably, we think that this mechanism might play a critical role also in the bulk LC phases where the comproportionation reaction might occur via a hopping mechanism through the LC film, thereby affecting the charge carrier mobility and consequently, electrochromism and electrofluorescence properties.[12]

In conclusion, the *mV(NTf₂)₂* are an important class of ionic liquid crystals with multifunctional properties. They are electroactive with n-type character and have a energy LUMO level very close to that of other n-type organic semiconductors. They are also strongly fluorescence and electrochromic. For these reasons, it is anticipated that they might be used as electron-acceptors materials for several applications in organic electronics.

Notes and references

*ᵃDepartment of Chemistry and Chemical Technologies, University of Calabria, Via P. Bucci, Arcavacata di Rende (CS) 87036, Italy

ᵇInstitute of Chemistry, Military University of Technology, Kaliskiego 2, 00-908 Warsaw, Poland.

ᶜFaculty of Chemistry, University of Warsaw, Zwirki i Wigury 101, 02-089 Warsaw, Poland.

E-mail: sante.cospito@unical.it, amerigo.beneduci@unical.it*

†Electronic Supplementary Information (ESI) available: Synthetic route of the compounds, DSC diagrams of *8V(NTf₂)₂*, POM images of *12V(NTf₂)₂* at 166 °C and 180 °C in the 1ˢᵗ heating scan and upon cooling from IL state at 130 °C and 68 °C, POM images of a thin film of *12VI₂* between two glass slides under cross polarized, at 250 °C, 240 °C and at 225 °C on cooling from the IL state, X-ray diffractogram of *12V(NTf₂)₂* at 140 °C and schematic illustration of the Colᵣ C2/m mesophase, XRD diffractograms of *12VI₂* recorded at 160 °C on the 1ˢᵗ heating scan and at 230 °C on the 1ˢᵗ cooling scan, plot of the melting point *vs.* alkyl chain length for the two thienoviologen homologous series, cyclic voltammograms at different scan rates of *12V(NTf₂)₂* (0.5 mM) in electrolyte solution PC/0.1 M TBAPF₆ with and without Fc/Fc⁺. See DOI: 10.1039/b000000x/

1   K. Binnemans, *Chem. Rev.*, 2005, **105**, 4148.

2   N. Yamanaka, R. Kawano, W. Kubo, N. Masaki, T. Kitamura, Y. Wada, M. Watanabe and S. Yanagida, *J. Phys. Chem. B*, 2007, **111**, 4763.

3   R. Kawano, M. K. Nazeeruddin, A. Sato, M. Grätzel and M. Watanabe, *Electrochem. Commun.*, 2007, **9**, 1134.

4   A. Abate, A. Petrozza, G. Cavallo, G. Lanzani, F. Matteucci, D. W. Bruce, N. Houbenov, P. Metrangolo and G. Resanti, *J. Mater. Chem. A*, 2013, 1, 6572.

5   D. Högberg, B. Soberats, S. Uchida, M. Yoshio, L. Kloo, H. Segawa and T. Kato, *Chem. Mater.*, 2014, **26**, 6496.

6   T. Kato, *Angew. Chem. Int. Ed*. 2010, **49**, 7847.

7   J. Sakuda et al. *Adv. Function. Mater.*, 2015, **25**, 1206.

8   B. Soberats, E. Uchida, M. Yoshio, J. Kagimoto, H. Ohno and T. Kato, *J. Am. Chem. Soc.*, 2014, **136**, 9552.

9   S. Chen and S. H. Eichlhorn, Isr. J. Chem. 2012, **52**, 830.

10 S. Yazaki, M. Funahashi and T. Kato, *J. Am. Chem. Soc.*, 2008, **130**, 13206.

11 S. Yazaki, M. Funahashi, J. Kagimoto, H. Ohno and T. Kato, *J. Am. Chem. Soc.*, 2010, **132**, 7702.

12 A. Beneduci, S. Cospito, M. La Deda, L. Veltri and G. Chidichimo, *Nat. Commun.,* 2014, 5:3105 DOI: 10.1038/ncomms4105.

13 Isoda k., Yasuda T., Kato T., *J. Mater. Chem.* 2008, **18**, 4522.

14 T. Yasuda, H. Ooi, J. Morita, Y. Akama, K. Minoura, M. Funahashi, T. Shimomura and T. Kato, *Adv. Funct. Mater.* 2009, **19**, 411.

15 A. E. Murschell, W. H. Kan, V. Thangadurai and T. Sutherland, *Phys. Chem. Chem. Phys.* 2012, **14**, 4626.

16 P. M. S. Monk in *The viologens: physico-chemical properties, synthesis and applications of the salts of 4,4'-bipyridine*, Wiley-VCH: Weinheim, England, 1998.

17 P. M. S. Monk, , R. J. Mortimer and D. R. Rosseinsky in *Electrochromism: Fundamentals and Applications*, Wiley-VCH, Weinheim, England, 1995.

18 R. J. Mortimer, A. L. Dyer and J. R. Reynolds, *Displays*, 2006, **27**, 2.

19 P. K. Bhowmik, H. Han, I. K. Nedeltchev, and J. Cebe, *Mol. Cryst. Liq. Cryst.*, 2004, **419**, 27.

20 V. Causin and G. Saielli, *J. Mol. Liq.*, 2009, **145**, 41.

21 V. Causin V and G. Saielli, *J. Mater. Chem.*, 2009, **19**, 9153.

22 G. Casella, V. Causin F. Rastrelli and G. Saielli, *Phys. Chem. Chem. Phys.,* 2014, **16**, 5048.

23 K. Tanabe, T. Yasuda, M. Yoshio and T. Kato *Org. Lett.*, 2007, **9**, 4271.

24 S. Asaftei, M. Ciobanu, A. M. Lepadatu, E. Song and U. Beginn, *J. Mater. Chem.*, 2012, **22**, 14426.

25 K. Takahashi, T. Nihira, K. Akiyama, Y. Ikegami, and E. Fukuyo, *J. Chem. Soc. Chem. Commun.* 1992, 620.

26 M. Valášek, J. Pecka, J. Jindřich, G. Calleja, P. R. Craig and J. Michl, *J. Org. Chem.* 2005, **70**, 405.

27 W. W. Porter III, T. P. Vaid and A. L. Rheingold, *J. Am. Chem. Soc.*, 2005, **127**, 16559.

28 S. Durben, and T. Baumgartner, *Angew. Chem. Int. Ed.,* 2011, **50**, 7948.

29 T. S. Arrhenius, M. Blanchard-Desce, M. Dvolaitsky, J. M. Lehn, and J. Malthete, *Proc. Natl. Acad. Sci.*, 1986, **83**, 5355.

30 W. M. Albers, J. O. Lekkala, L. Jeuken, G. W. Canters and A. P. F. Turner, *Bioelectrochem. Bioenerg.* 1997, **42**, 25.

31 W. M. Albers, J. Likonen, J. Peltonen, O. Teleman and H. Lemmetyinen, *Thin Solid Films* 1998, **330**, 114.

32 A. Beneduci, S. Cospito, A. Crispini, B. Gabriele, F. P. Nicoletta, L. Veltri, and G. Chidichimo, *J. Mater. Chem. C*, 2013, **1**, 2233.

33 J. Hock, A. M. W. Cargill Thompson, J. A. McCleverty, and M. D. Ward, *J. Chem. Soc., Dalton Trans.*, 1996 4257.

34 P. H. J. Kouwer and T. M. Swager, *J. Am. Chem. Soc.* **2007**, 129, 14042.

35 M. E. Alberto, B. C. De Simone, S. Cospito, D. Imbardelli, L. Veltri, G. Chidichimo, and N. Russo, *Chem. Phys. Lett.*, 2012, **552**, 141.

36 A. Beneduci, S. Cospito, M. La Deda and G. Chidichimo, *Adv. Funct. Mater.*, 2015, **25**, 1240.

37 M. Helbig and H.-H. Hörhold, *Makromol. Chem.*, 1993, **194**, 1607.

38 R. Cervini, X. C. Li, G. W. C. Spencer, A. B. Holmes, S. C. Moratti and R. H. Friend, *Synth. Met.* 1997, **84**, 359.

39 I. Seguy, P. Jolinat, P. Destruel, and J. Farenc, *J. Appl. Phys.*, 2001, **89**, 5442.

40 H.-J. Yen and G.-S. Liou, *Chem. Mater.* 2009, **21**, 4062.

41 C. J. Brabec, N. S. Sariciftci and J. C. Hummelen, *Adv. Funct. Mat.*, 2001, **11**, 15.

42 S. Sergeyev, W. Pisula and Y. H. Geerts, *Chem. Soc. Rev.*, 2007, **36**, 1902.

43 W. Pisula, M. Zorn, J. Y. Chang, K. Müllen and R. Zentel, *Macromol. Rapid Commun.*, 2009, **30**, 1179.

44 O' Neill and S. M. Kelly, *Adv. Mater.*, 2011, **23**, 566.

45 M. Funahashi, *J. Mater Chem. C*, 2014, **2**, 7451.

46 S. B. Meier, D. Tordera, A. Pertegás, C. Roldán-Carmona, E. Ortí and H. J. Bolink, *Mater. Today,* 2014, **17**, 217.

47 A. Beneduci, S. Cospito, D. Imbardelli, B. C. De Simone and G. Chidichimo, *Mol. Cryst. Liq. Cryst.*, 2015, In press.

48 B. Gao, L. Zhang, Q. Bai, Y. Li, J. Yang, L. Wang, *New J. Chem.*, 2010, **34**, 2735.

49 X.-Y. Liu, T. Usui and J. Hanna, *Chem. Eur. J.*, 2014, **20**, 14207.

50 J. Eccher, G. C. Faria, H. Bock, H. von Seggern and H. Bechtold, *ACS Appl. Mater. Interfaces*, 2013, **5**, 11935.

51 K. Isoda, T. Abe, M. Funhashi and M. Tadokoro, *Chem. Eur. J.*, 2014, **20**, 7232.

52 C. L. Chochos, N. Tagmatarchis and V. G. Gregoriou, *RSC Adv.*, 2013, **3**, 7160.

53 M.-A. Muth, G. Gupta, A. Wicklein, M. Carrasco-Orozco, T. Thurn-Albrecht and M. Thelakkat, *J. Phys. Chem. C,* 2014, **118**, 92.

54 M. Funahashi, A. Sonoda, *Phys. Chem. Chem. Phys.* 2014, **16**, 7754.